BIOCHEMISTRY
including biophysical chemistry & molecular biology

Article

pubs.acs.org/biochemistry

Host Cell Cytotoxicity and Cytoskeleton Disruption by CerADPr, an ADP-Ribosyltransferase of *Bacillus cereus* G9241

Nathan C. Simon,[†] James M. Vergis,[‡] Avesta V. Ebrahimi,[‡] Christy L. Ventura,[‡] Alison D. O'Brien,[‡] and Joseph T. Barbieri*[,†]

[†]Microbiology, Immunology, and Molecular Genetics, Medical College of Wisconsin, Milwaukee, Wisconsin 53226, United States
[‡]Microbiology and Immunology, Uniformed Services University of the Health Sciences, Bethesda, Maryland 20814, United States

Supporting Information

ABSTRACT: *Bacillus cereus* G9241 was isolated from a welder suffering from an anthrax-like inhalation illness. *B. cereus* G9241 encodes two megaplasmids, pBCXO1 and pBC210, which are analogous to the toxin- and capsule-encoding virulence plasmids of *Bacillus anthracis*. Protein modeling predicted that the pBC210 LF homologue contained an ADP-ribosyltransferase (ADPr) domain. This putative bacterial ADP-ribosyltransferase domain was denoted CerADPr. Iterative modeling showed that CerADPr possessed several conserved ADP-ribosyltransferase features, including an α-3 helix, an ADP-ribosyltransferase turn−turn loop, and a "Gln-XXX-Glu" motif. CerADPr ADP-ribosylated an ∼120 kDa protein in HeLa cell lysates and intact cells. EGFP-CerADPr rounded HeLa cells, elicited cytoskeletal changes, and yielded a cytotoxic phenotype, indicating that CerADPr disrupts cytoskeletal signaling. CerADPr(E431D) did not possess ADP-ribosyltransferase or NAD glycohydrolase activities and did not elicit a phenotype in HeLa cells, implicating Glu431 as a catalytic residue. These experiments identify CerADPr as a cytotoxic ADP-ribosyltransferase that disrupts the host cytoskeleton.

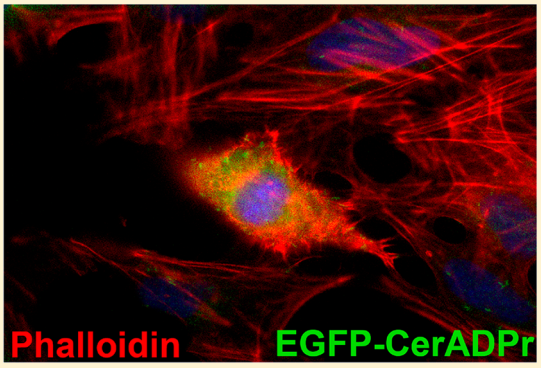

Bacterial ADP-ribosylating exotoxins (bAREs) catalyze the transfer of ADP-ribose from NAD to a target residue within a eukaryotic protein. This modification is primarily used as a mechanism of virulence by inactivating (or activating) host proteins, often leading to cell death. bAREs are usually categorized into one of four major groups based on their eukaryotic substrates:[1] Cholera toxin (CT)-like toxins modify heterotrimeric G-proteins,[2,3] diphtheria toxin (DT)-like toxins modify elongation factor 2,[4,5] C3-like exoenzymes modify small GTPases,[6−8] and the vegetative insecticidal protein-like (VIP) binary toxins modify actin.[9−12] C3 and VIP2 proteins share ADPr domain organization and structural conservation, despite different manners of substrate recognition.[13−15]

While limited amino acid sequence identity exists between the VIP2 and C3 transferases, there is strict conservation of critical residues required for ADP-ribosyltransferase activity. These residues have been designated the "RSE motif" and consist of three groups of residues (Arg, Ser-Thr-Ser, and Gln/Glu-XXX-Glu) located in discrete regions of the protein.[16] Together, these three motifs form the NAD binding pocket responsible for NAD hydrolysis and the transfer of the ADP-ribose moiety onto the substrate acceptor residue. Disruption of these residues, especially the invariant catalytic glutamic acid in the Gln/Glu-XXX-Glu motif, results in a nonfunctional enzyme. The primary structural elements of bARE ADP-ribosyltransferase domains have been designated A−F.[17] Region A is the first N-terminal α-helix and is responsible for recognition of the substrate by some bAREs, including ExoT recognition of CrkI/II.[17] Region B, helix α-3, is responsible for the stabilization of the active site glutamic acid and NAD and the positioning of the target residue. Region C, the ADP-ribosyltransferase−turn−turn (ARTT) loop, stabilizes the target residue and binds the N-ribose of NAD to create a conformation ideal for hydrolysis. Region E, the phosphate−nicotinamide loop, contains the conserved Ser-Thr-Ser motif and is responsible for the positioning of the catalytic Glu for proper NAD cleavage. Regions B, C, and E have also been implicated in bARE−substrate interactions.[13,14,17,18]

Recently, an in silico analysis was performed on known bacterial protein-encoding sequences to identify new bAREs through recognition of these conserved protein folding motifs.[19] This approach identified six new putative bAREs from diverse species, including *Vibrio cholerae*, *Enterococcus faecalis*, *Photorhabdus luminescens*, and *Bacillus cereus*. One putative toxin was identified from the genome of a clinical isolate of *B. cereus* (G9241). *B. cereus* is a Gram-positive spore-forming organism that is widely distributed in the environment and is the prototypical member of the *B. cereus* group, which includes *Bacillus thuringiensis* and *Bacillus anthracis*. The *B. cereus* group sharea high degree of genomic similarity; however,

Received: May 25, 2012
Revised: August 9, 2012
Published: August 30, 2012

dx.doi.org/10.1021/bi300692g | *Biochemistry* 2013, 52, 2309−2318

the disease phenotypes associated with the different species are widely varied. *B. cereus* infection is primarily associated with food-borne illness and opportunistic infection of immunocompromised individuals, while *B. anthracis* is the etiologic agent of anthrax, a disease that can be fatal to humans in cases of pulmonary or gastrointestinal infection.

Anthrax virulence is modulated by both encapsulation of the bacterium within an antiphagocytic poly-D-glutamate capsule and expression of anthrax toxin, a complex of three proteins: protective antigen (PA), lethal factor (LF), and edema factor (EF).[20] PA binds to a host receptor,[21−23] is processed by proteases,[24] and self-associates into heptamers[25,26] or octamers.[27,28] Multiple copies of LF, a potent MAPKK zinc metalloprotease,[29,30] or EF, an adenylate cyclase,[31,32] bind PA and enter through clathrin-mediated endocytosis.[33] Upon endosome acidification,[34,35] LF and EF cross the endosome membrane through the oligomeric PA pore and modify cellular signaling.[36]

Of recent concern, environmental *B. cereus* isolates that are responsible for serious illness and death have been isolated from otherwise healthy individuals, primarily welders and metalworkers.[37,38] Several *B. cereus* strains, including *B. cereus* G9241, have been implicated in a pulmonary anthrax-like disease, resulting in significant morbidity or death. Many of these *B. cereus* strains contain a homologue to *B. anthracis* pXO1, which encodes the anthrax toxin genes.[39] *B. cereus* G9241 contains two large plasmids, pBCXO1 (191 kb), a pXO1 homologue, and pBC210 (210 kb). pBCXO1 encodes the three subunits of *B. anthracis* anthrax toxin, consisting of *lef* (lethal factor, LF, 99% identical to *B. anthracis* LF), *cya* (edema factor, EF, 96% identical), and *pag* (protective antigen, PA, 98% identical), which are expressed in vitro.[40] pBC210 encodes additional copies of *pag* (60% identical) and *lef* (36% identical), as well as genes encoding the machinery required to create a polysaccharide capsule. Sequence analysis of pBC210 *lef* shows the presence of a putative PA binding domain but no coding sequence for the LF MAPKK metalloprotease domain (Figure 1 of the Supporting Information). Instead, a "VIP2-like domain" that comprises a putative ADP-ribosyltransferase domain that is homologous in sequence and structure to the binary ADP-ribosylating toxins is present.[19] The pBC210 *lef* gene product was originally denoted "Certhrax" because its sequence is similar to that of anthrax LF; however, we have chosen "Cereus toxin" to describe the full-length protein to remove any confusion with anthrax and lethal factor, while CerADPr will be used to denote the active ADP-ribosyltransferase domain. Iterative modeling of the crystal structure of CerADPr shows remarkable structural similarity of the LF PA binding domain and "VIP2-like" regions, indicating that they may share conserved structure and function. However, LF contains none of the conserved bacterial ADP-ribosyltransferase residues in the VIP2-like domain, which are present in CerADPr (Figure 1 of the Supporting Information).

Iterative BLAST analyses with the coding sequence of Cereus toxin (residues 1−476) returned high-scoring matches with multiple members of the VIP2-like and C3-like ADP-ribosyltransferases, including VIP2, Iota toxin, C3bot, and C3Cer. Sequence alignment of these bacterial ADP-ribosyltransferases shows very limited conservation of the N-terminal binding domain of Cereus toxin with the binding domains of Iota toxin and VIP2, while the ADP-ribosyltransferase domains of the five proteins show higher levels of conservation, with the "RSE" motif completely conserved (Figure 2 of the Supporting Information). Iterative structural modeling of CerADPr using Iota toxin as a template resulted in a model with a root-mean-square deviation of 2.8 Å for 170 Cα atoms. However, CerADPr contains an active site Gln-XXX-Glu motif, which is associated with C3 exoenzyme modification of Rho at Asn41.[41] These similarities prompted the analysis of Cereus toxin as a novel ADP-ribosyltransferase.

EXPERIMENTAL PROCEDURES

Plasmid Vectors and Mutagenesis. The gene encoding the ADP-ribosyltransferase domain of Cereus toxin (residues 226−476, predicted molecular mass of 29451 Da, termed CerADPr) was amplified and subcloned into pET15b (pET-CerADPr) (Novagen) and pEGFP-C3 (pEGFP-CerADPr) (Clontech). Site-directed mutagenesis generating an E431D mutation within CerADPr was performed using Quikchange site-directed mutagenesis (Agilent Technologies) with the following primers: + strand, 5′-GAATATCCAGGGCAATAT-GACATGTTAATAAATAG-3′; − strand, 5′-CTATTTAT-TAACATGTCATATTGCCCTGGATATTC-3′. Plasmids were transformed into *Escherichia coli* (TG1), and the DNA sequence was confirmed.

Expression and Purification of Recombinant Proteins. pET15-CerADPr and pET-CerADPr(E431D) were transformed into *E. coli* BL21(DE3). Cells were plated overnight at 37 °C with 250 μg/mL ampicillin. Cells were added to 400 mL of LB broth (Miller salts, BD Biosciences) with ampicillin and cultured for 2 h at 30 °C, after which 1 mM IPTG was added, and the cells were cultured overnight at 16 °C. Cells were harvested, suspended in binding buffer [20 mM Tris-HCl (pH 7.9), 500 mM NaCl, and 5 mM imidazole] with bacterial protease inhibitor cocktail (Sigma), RNase (20 μg/mL), and DNase (20 μg/mL), and broken with a French press. The lysate was centrifuged (30000*g* for 20 min) and the soluble fraction passed through a 0.45 μm filter. The filtrate was subjected to Ni^{2+} affinity resin chromatography (Qiagen). His(6) fusion proteins were eluted in binding buffer with 250 mM imidazole. The eluate was subjected to size-exclusion fractionation by Sephacryl S200 (Sigma) in 10 mM Tris-HCl (pH 7.6) and 20 mM NaCl. Peak fractions were dialyzed into 10 mM Tris-HCl (pH 7.6), 20 mM NaCl, and 40% glycerol and stored at −80 °C. A typical purification yielded ∼4 mg of CerADPr/L of culture. His(6)-ExoS(78−453) was purified as previously described.[42]

HeLa Cell Harvesting and Fractionation. HeLa cells (ATCC CCL-2) were cultured in MEM (Life Technologies) supplemented with 10% fetal calf serum, nonessential amino acids, sodium pyruvate, sodium bicarbonate, and penicillin/streptomycin and maintained humidified at 37 °C in 5% CO_2. Confluent plates (150 mm) of HeLa cells were washed (PBS) and scraped into 1 mL of HB buffer [200 mM sucrose, 3 mM imidazole, and mammalian protease inhibitor cocktail (Sigma)]. Cells were broken by 25−30 passes through a 26 gauge needle and then centrifuged at 1000*g* to pellet unbroken cells and nuclei. The supernatant (total lysate) was centrifuged at 100000*g* in a TLA100.3 rotor (Beckman) for 1.5 h at 4 °C. The supernatant (soluble) was stored at −80 °C. The pelleted membranes were suspended in PBS and 0.1% Triton X-100 (TX-soluble) and stored at −80 °C. Protein concentrations in each fraction (total lysate, soluble, and TX-soluble) were determined with a BCA assay (Pierce).

In Vitro ADP Ribosylation Assay. Reaction mixtures (50 μL) contained 10 mM Tris-HCl (pH 7.6), 20 mM NaCl, 50 μg

of HeLa lysate, 4 μM 6-biotin-17-NAD (Trevigen), and the indicated amount of CerADPr or ExoS. Reaction mixtures were incubated at room temperature (RT) for the indicated time and reactions stopped with Laemmli buffer and boiling. Reaction mixtures were subjected to sodium dodecyl sulfate−polyacrylamide gel electrophoresis (SDS−PAGE) and transferred to a polyvinylidene fluoride (PVDF, Millipore) membrane for immunoblot analysis.

Detection of Biotin-ADP-ribose. PVDF membranes were blocked for 30 min in PBS and 2% BSA and then incubated with a streptavidin−HRP conjugate (1:80000 final dilution; Pierce catalog no. 21130) for 1 h at RT. Luminescence from each lane was measured, with the most intense lane (ExoS-50 ng) set to 100%. An unpaired *t* test analysis was performed on columns with GraphPad Prism 5 (GraphPad Software Inc.) (*p < 0.05; **p < 0.01).

Detection of Host Proteins in the HeLa Cell Lysate. PVDF membranes were blocked for 30 min in TBST and 2% milk. Membranes were incubated with α-GFP IgG (mouse, 1:2000; Covance), α-β-actin IgG (mouse, 1:5000; Sigma), or α-tubulin antibody (rabbit, 1:5000; Abcam). Primary antibodies were detected with either goat α-mouse-HRP IgG (1:30000; Pierce) or goat α-rabbit-HRP IgG (1:30000; Pierce). Membranes were probed with Pico Super Signal (Pierce), and luminescence was measured with a CCD camera and AlphaView SA software (Cell Biosciences Inc.). Images were cropped in Photoshop (Adobe). Quantification of luminescence was performed with AlphaView software from a minimum of four independent experiments.

NAD Glycohydrolase Assay. This method was adapted from a thin-layer chromatography protocol in ref 43 in which 1.6 μM recombinant CerADPr, CerADPr(E431D), or ExoS was incubated with 2.5 mM NAD (Sigma) for 0−48 h at 37 °C. After the indicated time point, the reaction mixture was spotted onto poly(ethyleneimine)-cellulose (PEI-cellulose) TLC plates (Selecto Scientific) and resolved with 0.4 M LiCl. TLC plates were visualized under UV light and imaged with a CCD camera and AlphaView SA software (Cell Biosciences Inc.). Quantification of ADP-ribose generated from NAD was performed with AlphaView software from three independent experiments and normalized to a standard of ADP-ribose. An unpaired *t* test was performed to determine statistical significance (*p < 0.05; **p < 0.01).

Cell Culture and Transfection. HeLa cells were cultured to ∼70% confluence in 24-well plates and transfected with pEGFP-CerADPr, pEGFP-CerADPr(E431D), or pEGFP using Lipofectamine 2000 (Life Technologies) according to the manufacturer's protocol. At the indicated times, cells were washed twice with PBS and processed for immunofluorescence as described below. For the analysis of HeLa cell lysates, cells were cultured to ∼70% confluence in six-well plates and transfected with the indicated plasmid in Lipofectamine 2000 for either 5 or 20 h, scraped into 1 mL of HB, and lysed by 25−30 passages through a 26 gauge needle. Cell lysates were incubated with 25 μg of TX-soluble protein and 4 μM 6-biotin-17-NAD for 1 h at RT to assay for CerADPr activity, or the lysates were immediately resolved by SDS−PAGE and transferred to PVDF membranes for immunoblot analysis. The cytotoxic potential of CerADPr was measured in HeLa cells using a trypan blue exclusion assay,[44] with ExoS as a positive control, pExoS (RhoGAP−/ADPr+). Cells were transfected according to the manufacturer's protocol, and 5 and 20 h post-transfection (HPT), medium was removed and cells were washed and stained for 5 min with 0.4% trypan blue (Life Technologies). Trypan blue was removed; cells were washed in low-serum medium, and color images were obtained using a 10× objective and Retiga-2000R CCD camera (QImaging) with NIS Elements software (Nikon). Cytotoxicity was determined by counting the number of trypan blue positive HeLa cells per total number of HeLa cells per field. Five random fields were assayed, and the results of this determination are shown. Three biological replicates were performed for each time point. A one-way analysis of variance (ANOVA) was performed in GraphPad Prism 5 (GraphPad Software Inc.) (**p < 0.01).

HeLa Cell Permeabilization and Detection of Intracellular ADP Ribosylation. This protocol was adapted from ref 45. HeLa cells, transfected or nontransfected, were washed in 1 mL of ice-cold HGI buffer (20 mM PIPES, 2 mM Na-ATP, 4.8 mM magnesium acetate, 0.15 M potassium glutamate, 2 mM EGTA, and potassium hydroxide adjusted to pH 7.0) and then incubated for 15 min at 4 °C with 200 ng/mL tetanolysin (Santa Cruz Biotechnology) diluted in HGI. Cells were then incubated with HGI containing either 4 μM biotin-NAD (transfected cells) or 3 μg/mL recombinant protein (nontransfected cells) for 30 min at 37 °C. The buffer was then removed, and fresh serum-containing medium was added to seal membrane pores for 2 h. After incubation with biotin-NAD, transfected cells were lysed in RIPA buffer and Laemmli buffer was added. Lysate from cells incubated with recombinant protein was incubated with 50 ng of CerADPr and 4 μM biotin-NAD for an additional 1 h, followed by addition of Laemmli buffer and boiling. Samples were resolved by SDS−PAGE and subjected to immunoblot analysis.

Immunofluorescence Microscopy. HeLa cells were washed twice in PBS, $MgCl_2$, and $CaCl_2$ and then fixed with 4% paraformaldehyde in PBS for 15 min at RT. Cells were permeabilized with PBS, 0.1% Triton X-100, and 4% formaldehyde for 15 min and then incubated with 150 mM glycine for 15 min. Wells were blocked with PBS, 2.5% BSA, 10% FBS, 0.05% Tween 20, and 0.1% Triton X-100 for 1 h at RT and then incubated with primary antibody for 1 h at RT. Alexa Fluor647-phalloidin (Life Technologies; 1:1000 final dilution) was used to label the actin cytoskeleton, and rabbit α-tubulin IgG (Abcam; 1:2000 final dilution) followed by goat α-rabbit IgG Alexa Fluor568 (Life Technologies; 1:500 final dilution) labeled microtubules. Antibodies were diluted in PBS, 1% BSA, 5% FBS, 0.05% Tween 20, and 0.1% Triton X-100. After secondary antibody incubation, cells were washed three times with PBS and mounted with ProLong Gold antifade reagent (Life Technologies). Cells were viewed with a 60× oil immersion objective, and images were taken with a CoolSnap HQ CCD camera (Photometrics) and Metamorph (Molecular Devices) and processed with ImageJ (National Institutes of Health).

Structural Alignment Analysis. CerADPr (residues 226−476) was iteratively modeled on the ADP-ribosyltransferase domain (Ia) of Iota toxin, the top PSI-BLAST match for which a structure has been elucidated [Protein Data Bank (PDB) entry 1GIR)], using SWISSMODEL and Swiss-pdb-viewer version 4.02 (http://www.expasy.org/swissmod/SWISS-MODEL.html). ExoS (residues 234−453) was modeled as previously described.[17] Structural alignments of CerADPr, ExoS-ADPr, Iota toxin Ia, VIP2 (PDB entry 1QS2), C3Lim (PDB entry 3BW8 chain A), and C3bot (PDB entry 1G24 chain A) were performed with Visual Molecular Dynamics

Multiseq (http://www.ks.uiuc.edu/Research/vmd/, University of Illinois, Urbana, IL).[46]

RESULTS

CerADPr Is a Functional ADP-Ribosyltransferase. Initial experiments addressed the ADP-ribosyltransferase capacity of the predicted ADP-ribosyltransferase domain of Cereus toxin (residues 226−476, termed CerADPr). Expression of His(6)-CerADPr in *E. coli* yielded an ∼30 kDa protein by SDS−PAGE. Potential host targets for ADP ribosylation were assessed using a postnuclear supernatant from HeLa cells, which was fractionated by ultracentrifugation to separate membranes from cytoplasm. CerADPr ADP-ribosylated a 120 kDa protein in the HeLa cell lysate and cell membrane fractions (Figure 1A) but did not ADP-ribosylate host proteins in the cytosol. ADP ribosylation was dependent upon the addition of biotin-NAD (-biotin) or CerADPr (-ADPr) to the reaction mixture. *Pseudomonas aeruginosa* ExoS was used as a positive control for ADP ribosylation; ExoS ADP-ribosylated multiple substrates in the HeLa cell lysate, cytosol, and cell membrane fractions. The level of ADP-ribosylated substrate increased with

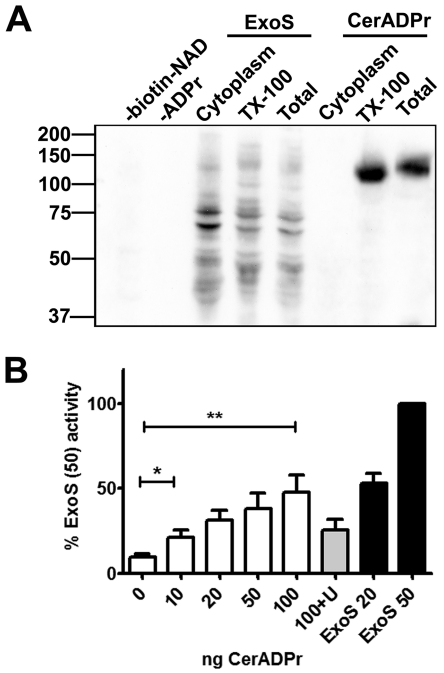

Figure 1. CerADPr selectively ADP-ribosylates a high-molecular mass host protein in HeLa cell membranes. (A) A HeLa cell lysate (Total) was centrifuged to generate cytosol (Cytoplasm) and membranes. Membranes were extracted with 0.1% Triton X-100 and centrifuged to remove the insoluble cell matrix (soluble membranes were termed Tx-100). Fractions were normalized for protein and incubated alone (-ADPr) or with 50 ng of CerADPr or 20 ng of ExoS for 1 h at 25 °C alone (-biotin-NAD) or with 4 μM biotin-NAD. The reaction mixture was subjected to SDS−PAGE, and proteins were transferred to a PVDF membrane, which was probed with streptavidin-conjugated HRP. (B) The Tx-100 HeLa cell fraction was incubated alone (0) or with the indicated amount of CerADPr (nanograms) or ExoS (nanograms) for 1 h at 25 °C with 4 μM biotin-NAD or with a 10-fold excess of unlabeled NAD (100 +U). The reaction mixture was treated as described above. The amount of biotin labeling from the 50 ng ExoS lane was set to 100%, and other signals were normalized (error bars display standard error of the mean). An unpaired t test was performed on selected columns (*p < 0.05; **p < 0.01).

increased concentrations of CerADPr (Figure 1B). Addition of unlabeled NAD reduced the amount of ADP ribosylation signal from biotin-NAD, supporting the specificity of CerADPr. The NAD glycohydrolase activity of CerADPr was compared to that of ExoS. CerADPr generated an increasing amount of ADP-ribose over time (Figure 2A). Little ADP-ribose was generated

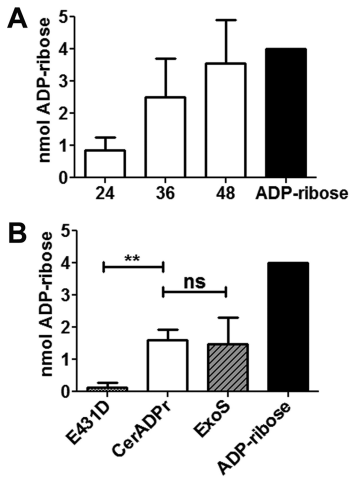

Figure 2. NAD glycohydrolase activity of CerADPr. (A) Recombinant CerADPr was incubated with 5 mM NAD^+ for 24, 36, or 48 h. An aliquot of each reaction mixture was analyzed by PEI-cellulose thin layer chromatography. (B) CerADPr, CerADPr(E431D), or ExoS was incubated with 5 mM NAD^+ for 24 h. An aliquot of each reaction mixture was then subjected to PEI-cellulose TLC. Plates were imaged, and the amount of ADP-ribose produced was quantified by densitometry and normalized to an ADP-ribose standard. Quantification is from three independent experiments, and error bars display the standard error of the mean. An unpaired t test was performed on selected columns (*p < 0.05; **p < 0.01).

when CerADPr(E431D) was incubated with NAD, supporting a role for E431 in catalysis. Quantification of ADP-ribose generated by the recombinant protein indicated that the glycohydrolase activity of CerADPr was within 2-fold of that of ExoS (Figure 2B).

CerADPr Contains a Conserved Bacterial ADP-Ribosyltransferase Motif and Active Site Glutamic Acid. Bacterial ADP-ribosyltransferases possess limited primary amino acid homology but contain three conserved regions within a conserved structural domain denoted the "RSE" motif.[16] The RSE motif forms the active site pocket and consists of a basic amino acid (Arg), a Ser-Thr-Ser motif present in the phosphate−nicotinamide (PN) loop, and an ADP-ribosyltransferase−turn−turn loop that includes a Gln/Glu-XXX-**Glu** motif that includes a catalytic glutamic acid (bold). Structural alignment with several bacterial ADP-ribosyltransferases showed that the RSE motif was conserved within CerADPr (Figure 3A). The PN loop of CerADPr, highlighted in orange, possesses a Ser-Thr-Ser motif within β-sheet 3, as well as a conserved aromatic residue forming the tail of the NAD-binding "scorpion" motif.[47] The structure of the ARTT loop (pink) was also conserved, which included α-helix 8 leading into the active site loop and β-sheet 6 containing the catalytic Glu. In addition, a highly charged and lysine-rich loop (Gly303−Glu315) is predicted from the model. This loop, termed the G-loop, is of unknown function and to the best of our knowledge is not present in other bAREs.

dx.doi.org/10.1021/bi300692g | *Biochemistry* 2013, 52, 2309−2318

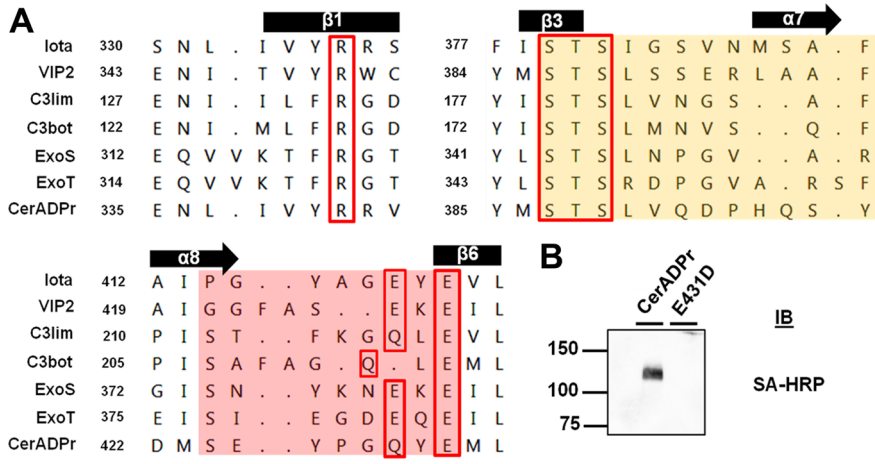

Figure 3. CerADPr domain with sequence and predicted structural conservation of other bacterial ADP-ribosyltransferases. (A) A predicted structure-based alignment of the Cereus toxin ADPr domain (CerADPr) was generated with the crystal structure of Iota toxin ADP-ribosyltransferase domain Ia (PDB entry 1GIR). Three regions of alignment that are common components of ADP-ribosyltransferase family members, including an Arg, the Ser-Thr-Ser motif, and the Gln/Glu-XXX-Glu sequence (RSE motif), are shown. The latter defines an active site glutamic acid that is conserved among ADP-ribosyltransferases. Secondary structure labeling is based off the Iota toxin Ia ADP-ribosyltransferase domain, starting with α-helix 1 of residues 214−232. (B) CerADPr(E431D) ADP-ribosyltransferase activity was measured relative to that of CerADPr by incubation with Tx-100 HeLa cell lysate and 4 μM biotin-NAD for 1 h at 25 °C. The reaction mixture was processed as described in the legend of Figure 1, and the ADP ribosylation of the high-molecular mass substrate is shown in the inset.

CerADPr contained the highest overall degree of similarity with VIP2 and Iota toxins but the highest degree of active site similarity with the C3 toxins that possess a Gln-XXX-Glu motif, rather than a Glu-XXX-Glu motif found in the binary actin ADP-ribosylating toxins and ExoS and ExoT. Site-directed mutagenesis of the predicted catalytic glutamic acid (Glu431) of CerADPr to aspartic acid (E431D) resulted in the loss of ADP ribosylation capacity (Figure 3B), consistent with Glu431 being the catalytic glutamic acid.[19]

CerADPr Disrupts the Host Cytoskeleton in HeLa Cells. To assess the effect of CerADPr on cell physiology, HeLa cells were transfected with pEGFP-CerADPr, pEGFP-CerADPr(E431D), or pEGFP and stained with phalloidin to examine the cellular actin architecture. By 4 h post-transfection (HPT), the earliest time that the EGFP signal was detectable, EGFP-CerADPr-transfected cells displayed an aberrant actin cytoskeleton (Figure 4A). EGFP-CerADPr-transfected cells showed a loss of actin stress fibers and formation of actin spikes at the cell periphery (Figure 4A, inset). At 5 HPT, cells rounded and did not possess defined actin stress fibers, and by 20 HPT, adherent EGFP fluorescent cells were not detected (data not shown). EGFP-CerADPr(E431D)-transfected HeLa cells had a normal actin cytoskeleton (Figure 4B), supporting a role for ADP ribosylation in the disruption of the actin cytoskeleton. Because CerADPr disrupted the actin cytoskeleton, the effect of CerADPr expression on the structure of microtubules was also examined by determining microtubule organization with α-tubulin immunostaining. At later incubation times, EGFP-CerADPr-transfected HeLa cells displayed disorganized microtubule architecture and the appearance of filamentous projections at the cell periphery, which stained positive for tubulin (data not shown). EGFP-CerADPr-(E431D)-transfected HeLa cells had a normal microtubule arrangement.

Because VIP2 family bAREs ADP-ribosylate actin to inhibit polymerization of actin microfilaments, the ability of CerADPr to ADP-ribosylate actin in HeLa cells was assessed. Western blotting of transfected cell lysates showed that transfection with

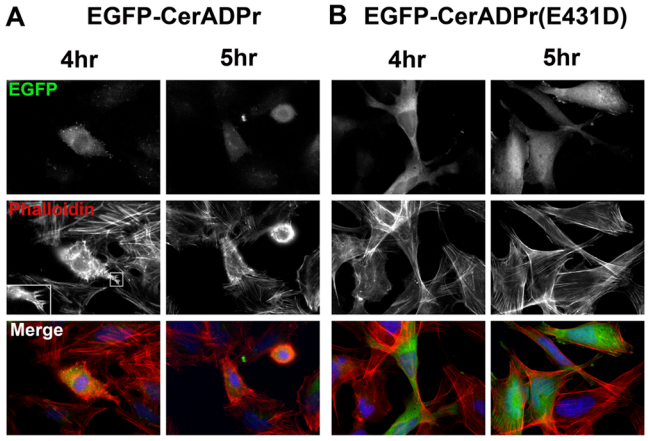

Figure 4. Expression of EGFP-CerADPr elicits early actin rearrangement in HeLa cells. HeLa cells were transfected with pEGFP-CerADPr (A) or pEGFP-CerADPr(E431D) (B) for 4 or 5 h when cells were fixed, permeabilized, and incubated with Alexa Fluor647-phalloidin to label the actin cytoskeleton. Cells were subjected to epifluorescence microscopy. Representative images are shown for each condition. The inset shows a close-up of actin spikes seen at the cell periphery of EGPF-CerADPr-transfected cells.

EGFP-CerADPr did not elicit a shift in the apparent electrophoretic mobility of either actin or tubulin, suggesting that expression of CerADPr did not directly modify either host protein (Figure 5A). The sequence similarity between CerADPr and C3Cer of *B. cereus* (Figure 2 of the Supporting Information) also prompted the determination of the ability of CerADPr to ADP-ribosylate Rho GTPases. However, under conditions where ExoS ADP-ribosylated Rab5, CerADPr did not ADP-ribosylate detectable amounts of Rho GTPases (Figure 3 of the Supporting Information).

Western blotting showed that EGFP-CerADPr(E431D)-transfected HeLa cell lysate possessed a GFP reactive protein with the expected molecular mass of an EGFP-CerADPr fusion (Figure 5A). A GFP reactive protein was not detected by

dx.doi.org/10.1021/bi300692g | *Biochemistry* 2013, 52, 2309−2318

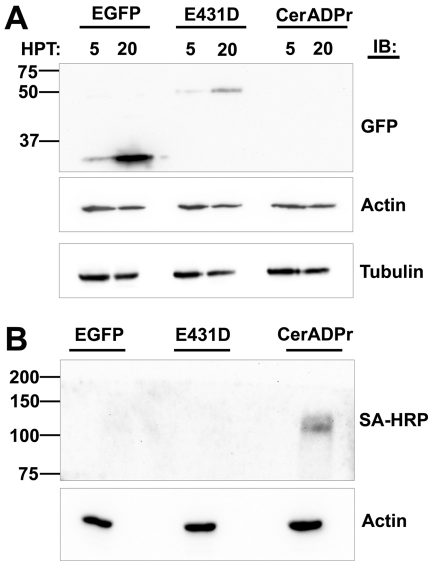

Figure 5. CerADPr does not covalently modify actin or tubulin. (A) HeLa cells were transfected with either pEFGP, pEGFP-CerADPr-(E431D), or pEGFP-CerADPr. At 5 and 20 HPT, cells were harvested and subjected to SDS−PAGE. The gel was transferred to PVDF membranes and probed independently with α-GFP, α-actin, and α-tubulin primary antibodies. Membranes were processed as described in the legend of Figure 1. (B) Cell lysates were prepared from HeLa cells transfected with either pEFGP, pEGFP-CerADPr(E431D), or pEGFP-CerADPr and incubated with the TX-100-soluble membrane fraction of HeLa cells and biotin-NAD. After 2 h, the reaction mixture was subjected to SDS−PAGE and proteins were transferred to PVDF membranes and probed for the ADP ribosylation of the high-molecular mass substrate of CerADPr and actin reactivity measured to normalize the cell lysates.

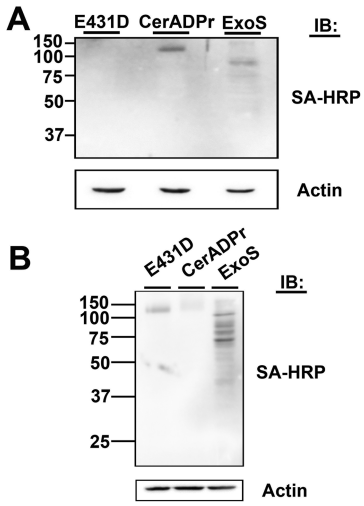

Figure 6. CerADPr ADP-ribosylates the 120 kDa target within HeLa cells. (A) HeLa cells were transfected with pEGFP-CerADPr, pEGFP-CerADPr(E431D), or pExoS for 2 h. Cells were treated with 200 ng/mL tetanolysin and then incubated with biotin-NAD for 2.5 h. Cell lysates were resolved by SDS−PAGE, and the incorporation of biotin-ADP-ribose was visualized by immunoblotting with streptavidin-HRP. Actin was used as a loading control. (B) HeLa cells were treated with 200 ng/mL tetanolysin and then incubated with 3 μg/mL recombinant CerADPr, CerADPr(E431D), or ExoS for 2 h. Cell lysates were prepared and then incubated with biotin-NAD and recombinant CerADPr for 1 h. Lysates were resolved by SDS−PAGE and transferred to PVDF membranes, where biotin-ADP-ribose incorporation was visualized with streptavidin-HRP. Actin was used as a loading control.

immunoblot in the lysates of EGFP-CerADPr-transfected HeLa cells, although intracellular expression of bAREs reduces the level of host protein expression.[44] Additionally, the lysate from cells transfected with pEGFP-CerADPr ADP-ribosylated the previously observed high-molecular mass host protein in HeLa cell lysates (Figure 5B), confirming that EGFP-CerADPr was expressed in the transfected HeLa cells.

CerADPr ADP-Ribosylates a 120 kDa Protein in HeLa Cells. To determine if CerADPr ADP-ribosylates the 120 kDa protein within intact HeLa cells, tetanolysin was used to reversibly generate pores in the plasma membrane to allow diffusion of externally added molecules into the cell.[48−50] HeLa cells transfected with EGFP-CerADPr, EGFP-CerADPr-(E431D), or ExoS were incubated with tetanolysin and biotin-NAD. Lysates from cells transfected with EGFP-CerADPr showed the ADP ribosylation of the 120 kDa protein, while lysates from cells transfected with EGFP-CerADPr(E431D) did not contain detectable ADP-ribosylated proteins (Figure 6A). Lysates from cells transfected with ExoS showed multiple ADP-ribosylated proteins, consistent with the ADP-ribosyltransferase specificity of this protein.

To corroborate the ability of CerADPr to ADP-ribosylate the 120 kDa protein in HeLa cells, a back ADP ribosylation experiment was performed. HeLa cells were incubated with tetanolysin and then incubated with recombinant CerADPr or CerADPr(E431D). Cell lysates from these cells were then incubated with recombinant CerADPr and biotin-NAD to ADP-ribosylate accessible 120 kDa protein. Lysates from cells incubated with CerADPr(E431D) possessed accessible 120 kDa protein for ADP ribosylation, while lysates from cells incubated with CerADPr possessed a reduced amount of accessible 120 kDa protein for ADP ribosylation (Figure 6B). This indicated that CerADPr had ADP-ribosylated the 120 kDa protein within HeLa cells.

CerADPr Is Cytotoxic for HeLa Cells. To determine if CerADPr was cytotoxic, HeLa cells were transfected with pEGFP-CerADPr, pEGFP-CerADPr(E431D), or pExoS-(R146K), a RhoGAP$^-$/ADPr+ ExoS derivative, and scored for trypan blue exclusion. ExoS was used as a positive control for cytotoxicity.[44] Trypan blue is excluded from viable cells but enters necrotic or apoptotic cells. At 5 HPT, ∼10% of cells transfected with pExoS were trypan blue positive, while at 20 HPT, ∼50% of transfected cells were trypan blue positive (Figure 7). At 5 HPT, ∼15% of pEGFP-CerADPr-transfected cells were trypan blue positive, and at 20 HPT, ∼45% of transfected cells were trypan blue positive. Cells transfected with pEGFP-CerADPr(E431D) showed limited numbers of trypan blue positive cells (∼15% at 20 HPT). This indicated that expression of CerADPr elicits a cytotoxic response in HeLa cells.

■ DISCUSSION

In silico structural analyses are powerful tools for discovering candidate bacterial virulence factors by predicting conservation of enzymatic folding motifs or catalytic residues within open reading frames from newly sequenced bacterial genomes. In this study, the predicted ORF of Cereus toxin (Certhrax) from *B. cereus* G9241 is shown to be a functional ADP-ribosyltransferase. CerADPr contained a conserved bacterial ADP-ribosyltransferase RSE motif in which mutation of the

dx.doi.org/10.1021/bi300692g | *Biochemistry* 2013, 52, 2309−2318

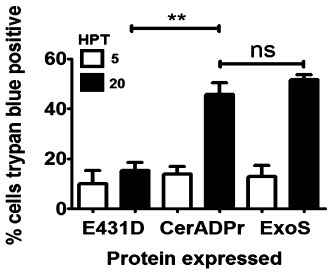

Figure 7. CerADPr is cytotoxic for HeLa cells. HeLa cells were grown to ∼70% confluence in six-well dishes and transfected with 500 ng of either pExoS, pEGFP-CerADPr(E431D), or pEGFP-CerADPr. At 5 and 20 HPT, medium was removed and cells were washed and stained for 5 min with trypan blue. Trypan blue was removed; cells were washed, and color images were obtained as described in Experimental Procedures. Cytotoxicity was determined by counting the number of trypan blue positive HeLa cells per total number of HeLa cells per field. Five random fields were assayed from three biological replicates, and the results of this determination are shown. One-way ANOVA was performed on all columns (**$p < 0.01$).

predicted conserved, invariant Glu resulted in a loss of ADP-ribosyltransferase activity. CerADPr targeted actin polymerization at early expression time points. However, these effects appeared to be off-target, because direct modification or loss of either actin or tubulin was not detected. CerADPr displayed a cytotoxic phenotype with temporal properties similar to those of ExoS, a known cytotoxic effector.[44]

Bacterial ADP-ribosyltransferase exotoxins (bAREs) have limited amino acid sequence identity, with conservation of structure and sequence active site motifs. The canonical bARE domain contains an RSE motif, consisting of Arg, Ser-Thr-Ser, and Gln/Glu-XXX-Glu motifs, except in the diphtheria toxin/Exotoxin A subfamily.[16] bAREs within the VIP2 or C3 subfamilies contain two additional structures, the phosphate−nicotinamide loop and helix α-3, which are absent in the cholera toxin-like bAREs.[51] Sequence and structural alignment with other bAREs showed that CerADPr had a conserved RSE motif, as well as the PN loop and helix α-3, as in members of the VIP2-like or C3-like bARE groups. Unexpectedly, CerADPr also contains an additional 12-residue loop (Gly303−Glu315), which, to the best of our knowledge, is not present in other bAREs. This loop, termed the G-loop, is of unknown function and highly charged with lysine residues.

Alignment of CerADPr with previously characterized bAREs yielded several dichotomies. The protein organization shows homology to the VIP2 subfamily of binary toxins, which ADP-ribosylate actin.[12] CerADPr had the highest-scoring PSI-BLAST match with Iota toxin from *Clostridium perfringens* and showed similarity to the binary actin-ADP-ribosylating VIP2. However, the presence of a Gln-XXX-Glu motif, rather than a Glu-XXX-Glu motif, in the ARTT loop implied that CerADPr may ADP-ribosylate targets in a manner similar to that of the C3 exoenzymes. A C3-like mechanism cannot be ruled out, as TccC5, a bARE from *Photorhabdus luminescens*, contains a Gln-XXX-Glu motif and ADP-ribosylates Gln61/63 of host Rho proteins, despite limited homology to the C3 exoenzymes.[52] However, in vitro ADP ribosylation assays showed that CerADPr does not ADP-ribosylate the Rho GTPases (Figure 3 of the Supporting Information). Because the target of CerADPr is detergent-solubilized from cellular membranes, the substrate of CerADPr may be an integral membrane protein, or a part of a membrane-associated complex. The sequence and structural duality suggests that CerADPr may belong to a new subfamily of bAREs with unique substrate specificity, because CerADPr ADP-ribosylates a 120 kDa target in eukaryotic cell lysates. Further, despite similarities in sequence and structure between CerADPr and the VIP2-like toxin subfamily members, CerADPr does not appear to directly modify actin either in vitro (Figure 1A) or in HeLa cells (Figure 5A). In other bAREs, mutation of the conserved, invariant Glu correlates with a >10000-fold reduction in ADP-ribosyltransferase activity.[53,54] While precise kinetic calculations are difficult without the identity of the substrate, CerADPr-(E431D) displayed limited cytotoxicity for HeLa cells and no ADP ribosylation of the 120 kDa substrate in vitro, as well as a loss of detectable NAD glycohydrolase activity.

Most bAREs target the cytoskeleton, either directly, through actin ADP ribosylation, or indirectly, by interfering with cytoskeletal signaling pathways. VIP2-like toxins and C3 exoenzymes disrupt actin filament polymerization, resulting in rounding and cell death, while other bAREs like ExoS or ExoT disrupt signaling by ADP-ribosylating ezrin/radixin/moesin proteins or CrkI/II, respectively.[13,55−58] These modifications alter cytoskeleton dynamics and result in cell rounding. CerADPr appears to share a similar ability to disrupt the cytoskeleton, causing stress fiber rearrangement and formation of actin spikes at the cell periphery early, followed by cell rounding and detachment from the growth surface with longer incubations. Formation of actin spikes is somewhat similar to effects induced by the *E. coli* effector Map, a Cdc42 guanine nucleotide exchange factor, which causes the formation of filapodia in intoxicated cells.[59,60] Current studies are directed toward resolving the identity of the 120 kDa host target that is ADP-ribosylated by Cereus toxin.

CerADPr disrupted microtubule structure, with filamentous projections extending from the periphery of cells displaying disrupted actin architecture, although microtubule disruption was observed only at longer incubation times. This phenotype has previously been observed in cells intoxicated with actin ADP-ribosylating binary toxin CDTa from *Clostridium difficile* and is thought to be a result of depolymerization of the F-actin cytoskeleton.[61] Therefore, it is likely the tubulin projections elicited by CerADPr result from actin depolymerization, because the extensions were observed upon extended incubations, after actin rearrangements were observed. Many bAREs, including the VIP2-like and C3-like bAREs, also stimulate a cytotoxic phenotype following cytoskeletal disruption, with ExoT and heat-labile enterotoxin being notable exceptions.[17,44,62−64] The CerADPr phenotype, then, appears to be similar to that of the VIP2 or C3 bAREs, despite the inability of CerADPr to directly ADP-ribosylate actin or the Rho proteins in vitro or in cell culture.

B. cereus pathogenesis is typically characterized by expression of various enterotoxins and hemolysins, resulting in mild to moderate gastroenteritis and emetic or diarrheal illness. However, several recently isolated *B. cereus* strains, including G9241, contain homologues of *B. anthracis* plasmid pXO1 that encode the three anthrax toxin components.[39] G9241 produces these proteins in vitro, and their expression is required for full virulence, as is the production of both a hyaluronic acid capsule[40] and a polysaccharide capsule.[40,65] Pulmonary anthrax-like disease observed in individuals infected with *B. cereus* G9241 may be due to the effects of the anthrax toxin homologues, acting via a mechanism similar to that of *B. anthracis* anthrax toxin. However, G9241 also contains a second

dx.doi.org/10.1021/bi300692g | *Biochemistry* 2013, 52, 2309−2318

large plasmid, encoding a novel ADP-ribosyltransferase, Cereus toxin (Certhrax). Other *B. cereus* strains encode bAREs, such as C3Cer or VIP2, but the pathogenic contributions of these proteins have not been well elucidated in mammals. Cereus toxin may contribute to *B. cereus* G9241 pathogenesis in an antiphagocytic capacity, either through disruption of actin polymerization or through its cytotoxic activity. Other bAREs studied in mammalian models, such as *Salmonella* SpvB, induce cytotoxicity in macrophages within 24 h of bacterium phagocytosis.[66] Alternatively, Cereus toxin could play a limited role in mammalian pathogenesis and be more directed toward environmental targets, like the crystal toxins expressed by *B. thuringiensis*, which primarily target insects. However, while considered an insect pathogen, *B. thuringiensis* has been associated with isolated cases of wound infection, food poisoning, and catheter-associated infections in immunocompromised humans.[67−69]

The sequence homology with the PA binding domain of lethal factor (Figure 1 of the Supporting Information) suggests that Cereus toxin could utilize a clathrin-dependent cell entry mechanism, similar to that employed by LF, although whether the entry mechanism and host receptor are identical or divergent needs to be explored.[22,33] Alternatively, the similarities with the VIP2-like binary toxins could implicate an entry mechanism similar to that of either Iota or C2, each of which utilizes a clathrin-independent pathway, or a clathrin-dependent pathway involving the Rho proteins.[70,71]

Dissecting the mechanisms behind novel bARE activity may lead to an effective strategy for neutralizing the virulence of a wide range of bacterial pathogens, while avoiding off-target effects on the host microbiome and development of resistance often observed with extended antibiotic therapy.[72−74] Unlike *B. anthracis*, *B. cereus* is naturally resistant to β-lactams, including cephalosporins, but currently responds well to other available antibiotics like vancomycin.[75,76] However, given the rise of multidrug resistance in other human pathogens, directed targeting of virulence factors is likely a safer long-term strategy for combatting these infections. Determination of the substrate and mechanism of Cereus toxin action may also lead to its use as a molecular tool in elucidating mammalian signaling pathways. Finally, understanding the activity of Cereus toxin will broaden our understanding of the pathogenesis of *B. cereus* G9241 and may lead to therapies for addressing the severe morbidities and mortality associated with emerging pathogenic strains of *B. cereus*.

■ ASSOCIATED CONTENT

Supporting Information

An amino acid homology alignment of CerADPr/lethal factor protein domains and a homology alignment of CerADPr with other bacterial ADP-ribosyltransferases as well as data showing the inability of CerADPr to ADP-ribosylate Rho proteins. This material is available free of charge via the Internet at http://pubs.acs.org.

■ AUTHOR INFORMATION

Corresponding Author

*Phone: (414) 955-8412. Fax: (414) 955-6535. E-mail: jtb01@mcw.edu.

Funding

J.T.B. acknowledges membership in the GLRCE and support by 1-U54-AI-057153 from the Region V Great Lakes Regional Center of Excellence, the National Institute of Allergy and Infectious Diseases (NIAID), and the National Institutes of Health Regional Center of Excellence for Biodefense and Emerging Infectious Diseases Research Program. N.C.S. was supported by NIAID Grant AI-AI30162. A.D.O. acknowledges support from the Biological Defense Research Directorate of the Naval Medical Research Center.

Notes

The authors declare no competing financial interest.

■ ACKNOWLEDGMENTS

We acknowledge the assistance of Amanda Przedpelski for protein production. The opinions expressed here are those of the authors and do not reflect the views of the United States Navy or the Department of Defense.

■ ABBREVIATIONS

ADPr, ADP-ribosyltransferase; bAREs, bacterial ADP-ribosylating exotoxins; CT, cholera toxin; DT, diphtheria toxin; VIP, vegetative insecticidal protein; PA, protective antigen; LF, lethal factor; EF, edema factor; CerADPr, Cereus toxin ADP-ribosyltransferase domain; PVDF, polyvinylidene fluoride.

■ REFERENCES

(1) Krueger, K. M., and Barbieri, J. T. (1995) The family of bacterial ADP-ribosylating exotoxins. *Clin. Microbiol. Rev. 8* (1), 34−47.

(2) Gill, D. M., and Meren, R. (1978) ADP-ribosylation of membrane proteins catalyzed by cholera toxin: Basis of the activation of adenylate cyclase. *Proc. Natl. Acad. Sci. U.S.A. 75* (7), 3050−3054.

(3) Moss, J., et al. (1979) NAD-dependent ADP-ribosylation of arginine and proteins by *Escherichia coli* heat-labile enterotoxin. *J. Biol. Chem. 254* (14), 6270−6272.

(4) Collier, R. J. (1967) Effect of diphtheria toxin on protein synthesis: Inactivation of one of the transfer factors. *J. Mol. Biol. 25* (1), 83−98.

(5) Van Ness, B. G., Howard, J. B., and Bodley, J. W. (1980) ADP-ribosylation of elongation factor 2 by diphtheria toxin. Isolation and properties of the novel ribosyl-amino acid and its hydrolysis products. *J. Biol. Chem. 255* (22), 10717−10720.

(6) Braun, U., et al. (1989) Purification of the 22 kDa protein substrate of botulinum ADP-ribosyltransferase C3 from porcine brain cytosol and its characterization as a GTP-binding protein highly homologous to the rho gene product. *FEBS Lett. 243* (1), 70−76.

(7) Coburn, J., et al. (1989) Several GTP-binding proteins, including p21c-H-ras, are preferred substrates of *Pseudomonas aeruginosa* exoenzyme S. *J. Biol. Chem. 264* (15), 9004−9008.

(8) Aktories, K., et al. (1989) The rho gene product expressed in *E. coli* is a substrate of botulinum ADP-ribosyltransferase C3. *Biochem. Biophys. Res. Commun. 158* (1), 209−213.

(9) Han, S., et al. (1999) Evolution and mechanism from structures of an ADP-ribosylating toxin and NAD complex. *Nat. Struct. Mol. Biol. 6* (10), 932−936.

(10) Aktories, K., et al. (1986) Botulinum C2 toxin ADP-ribosylates actin. *Nature 322* (6077), 390−392.

(11) Schering, B., et al. (1988) ADP-ribosylation of skeletal muscle and non-muscle actin by *Clostridium perfringens* iota toxin. *Eur. J. Biochem. 171* (1−2), 225−229.

(12) Vandekerckhove, J., et al. (1987) *Clostridium perfringens* iota toxin ADP-ribosylates skeletal muscle actin in Arg-177. *FEBS Lett. 225* (1−2), 48−52.

(13) Tsuge, H., et al. (2008) Structural basis of actin recognition and arginine ADP-ribosylation by *Clostridium perfringens* ι-toxin. *Proc. Natl. Acad. Sci. U.S.A. 105* (21), 7399−7404.

(14) Han, S., et al. (2001) Crystal structure and novel recognition motif of Rho ADP-ribosylating C3 exoenzyme from *Clostridium*

botulinum: Structural insights for recognition specificity and catalysis. *J. Mol. Biol. 305* (1), 95−107.
(15) Tsuge, H., et al. (2003) Crystal Structure and Site-directed Mutagenesis of Enzymatic Components from *Clostridium perfringens* Iota-toxin. *J. Mol. Biol. 325* (3), 471−483.
(16) Domenighini, M., and Rappuoli, R. (1996) Three conserved consensus sequences identify the NAD-binding site of ADP-ribosylating enzymes, expressed by eukaryotes, bacteria and T-even bacteriophages. *Mol. Microbiol. 21* (4), 667−674.
(17) Sun, J., et al. (2004) How bacterial ADP-ribosylating toxins recognize substrates. *Nat. Struct. Mol. Biol. 11* (9), 868−876.
(18) Wilde, C., et al. (2000) Recognition of RhoA by *Clostridium botulinum* C3 Exoenzyme. *J. Biol. Chem. 275* (22), 16478−16483.
(19) Fieldhouse, R. J., et al. (2010) Cholera- and Anthrax-Like Toxins Are among Several New ADP-Ribosyltransferases. *PLoS Comput. Biol. 6* (12), e1001029.
(20) Little, S. F., and Ivins, B. E. (1999) Molecular pathogenesis of *Bacillus anthracis* infection. *Microbes Infect. 1* (2), 131−139.
(21) Escuyer, V., and Collier, R. J. (1991) Anthrax protective antigen interacts with a specific receptor on the surface of CHO-K1 cells. *Infect. Immun. 59* (10), 3381−3386.
(22) Bradley, K. A., et al. (2001) Identification of the cellular receptor for anthrax toxin. *Nature 414* (6860), 225−229.
(23) Scobie, H. M., et al. (2003) Human capillary morphogenesis protein 2 functions as an anthrax toxin receptor. *Proc. Natl. Acad. Sci. U.S.A. 100* (9), 5170−5174.
(24) Singh, Y., et al. (1994) The chymotrypsin-sensitive site, FFD315, in anthrax toxin protective antigen is required for translocation of lethal factor. *J. Biol. Chem. 269* (46), 29039−29046.
(25) Milne, J. C., et al. (1994) Anthrax protective antigen forms oligomers during intoxication of mammalian cells. *J. Biol. Chem. 269* (32), 20607−20612.
(26) Petosa, C., et al. (1997) Crystal structure of the anthrax toxin protective antigen. *Nature 385* (6619), 833−838.
(27) Kintzer, A. F., et al. (2009) The Protective Antigen Component of Anthrax Toxin Forms Functional Octameric Complexes. *J. Mol. Biol. 392* (3), 614−629.
(28) Kintzer, A. F., et al. (2010) Role of the Protective Antigen Octamer in the Molecular Mechanism of Anthrax Lethal Toxin Stabilization in Plasma. *J. Mol. Biol. 399* (5), 741−758.
(29) Duesbery, N. S., Webb, C. P., Leppla, S. H., Gordon, V. M., Klimpel, K. R., Copeland, T. D., Ahn, N. G., Oskarsson, M. K., Fukasawa, K., Paull, K. D., and Vande Woude, G. F. (1998) Proteolytic inactivation of MAP-kinase-kinase by anthrax lethal factor. *Science 280*, 734−737.
(30) Duesbery, N. S., and Woude, G. F. V. (1999) Anthrax lethal factor causes proteolytic inactivation of mitogen-activated protein kinase kinase. *J. Appl. Microbiol. 87* (2), 289−293.
(31) Leppla, S. H. (1982) Anthrax toxin edema factor: A bacterial adenylate cyclase that increases cyclic AMP concentrations of eukaryotic cells. *Proc. Natl. Acad. Sci. U.S.A. 79* (10), 3162−3166.
(32) Leppla, S. H. (1984) *Bacillus anthracis* calmodulin-dependent adenylate cyclase: Chemical and enzymatic properties and interactions with eucaryotic cells. *Adv. Cyclic Nucleotide Protein Phosphorylation Res. 17*, 189−198.
(33) Abrami, L., et al. (2003) Anthrax toxin triggers endocytosis of its receptor via a lipid raft-mediated clathrin-dependent process. *J. Cell Biol. 160* (3), 321−328.
(34) Friedlander, A. M. (1986) Macrophages are sensitive to anthrax lethal toxin through an acid-dependent process. *J. Biol. Chem. 261* (16), 7123−7126.
(35) Gordon, V. M., Leppla, S. H., and Hewlett, E. L. (1988) Inhibitors of receptor-mediated endocytosis block the entry of *Bacillus anthracis* adenylate cyclase toxin but not that of *Bordetella pertussis* adenylate cyclase toxin. *Infect. Immun. 56* (5), 1066−1069.
(36) Miller, C. J., Elliott, J. L., and Collier, R. J. (1999) Anthrax Protective Antigen: Prepore-to-Pore Conversion. *Biochemistry 38* (32), 10432−10441.
(37) Hoffmaster, A. R., et al. (2006) Characterization of *Bacillus cereus* Isolates Associated with Fatal Pneumonias: Strains Are Closely Related to *Bacillus anthracis* and Harbor *B. anthracis* Virulence Genes. *J. Clin. Microbiol. 44* (9), 3352−3360.
(38) Miller, J. M., et al. (1997) Fulminating bacteremia and pneumonia due to *Bacillus cereus*. *J. Clin. Microbiol. 35* (2), 504−507.
(39) Hoffmaster, A. R., et al. (2004) Identification of anthrax toxin genes in a *Bacillus cereus* associated with an illness resembling inhalation anthrax. *Proc. Natl. Acad. Sci. U.S.A. 101* (22), 8449−8454.
(40) Wilson, M. K., et al. (2011) *Bacillus cereus* G9241 Makes Anthrax Toxin and Capsule like Highly Virulent *B. anthracis* Ames but Behaves like Attenuated Toxigenic Nonencapsulated *B. anthracis* Sterne in Rabbits and Mice. *Infect. Immun. 79* (8), 3012−3019.
(41) Sekine, A., Fujiwara, M., and Narumiya, S. (1989) Asparagine residue in the rho gene product is the modification site for botulinum ADP-ribosyltransferase. *J. Biol. Chem. 264* (15), 8602−8605.
(42) Knight, D. A., and Barbieri, J. T. (1997) Ecto-ADP-ribosyltransferase activity of *Pseudomonas aeruginosa* exoenzyme S. *Infect. Immun. 65* (8), 3304−3309.
(43) Randerath, K., and Randerath, E. (1964) Ion-exchange chromatography of nucleotides on poly-(ethyleneimine)-cellulose thin layers. *J. Chromatogr., A 16* (0), 111−125.
(44) Pederson, K. J., and Barbieri, J. T. (1998) Intracellular expression of the ADP-ribosyltransferase domain of *Pseudomonas* exoenzyme S is cytotoxic to eukaryotic cells. *Mol. Microbiol. 30* (4), 751−759.
(45) Ahnert-Hilger, G., et al. (1992) Exocytosis from permeabilized bovine adrenal chromaffin cells is differently modulated by guanosine 5′-[γ-thio]triphosphate and guanosine 5′-[$\beta\gamma$-imido]triphosphate. Evidence for the involvement of various guanine nucleotide-binding proteins. *Biochem. J. 284* (2), 321−326.
(46) Humphrey, W., Dalke, A., and Schulten, K. (1996) VMD: Visual molecular dynamics. *J. Mol. Graphics 14* (1), 33−38.
(47) Lee, Y.-M., et al. (2010) Conserved Structural Motif for Recognizing Nicotinamide Adenine Dinucleotide in Poly(ADP-ribose) Polymerases and ADP-Ribosylating Toxins: Implications for Structure-Based Drug Design. *J. Med. Chem. 53* (10), 4038−4049.
(48) Riese, M. J., et al. (2002) Auto-ADP-ribosylation of *Pseudomonas aeruginosa* ExoS. *J. Biol. Chem. 277* (14), 12082−12088.
(49) Riese, M. J., and Barbieri, J. T. (2002) Membrane Localization Contributes to the In Vivo ADP-Ribosylation of Ras by *Pseudomonas aeruginosa* ExoS. *Infect. Immun. 70* (4), 2230−2232.
(50) Walev, I., et al. (2001) Delivery of proteins into living cells by reversible membrane permeabilization with streptolysin-O. *Proc. Natl. Acad. Sci. U.S.A. 98* (6), 3185−3190.
(51) Holbourn, K. P., Shone, C. C., and Acharya, K. R. (2006) A family of killer toxins. *FEBS J. 273* (20), 4579−4593.
(52) Lang, A. E., et al. (2010) *Photorhabdus luminescens* Toxins ADP-Ribosylate Actin and RhoA to Force Actin Clustering. *Science 327* (5969), 1139−1142.
(53) Visschedyk, D. D., et al. (2010) Photox, a Novel Actin-targeting Mono-ADP-ribosyltransferase from *Photorhabdus luminescens*. *J. Biol. Chem. 285* (18), 13525−13534.
(54) Radke, J., Pederson, K. J., and Barbieri, J. T. (1999) *Pseudomonas aeruginosa* Exoenzyme S Is a Biglutamic Acid ADP-Ribosyltransferase. *Infect. Immun. 67* (3), 1508−1510.
(55) Maresso, A. W., Baldwin, M. R., and Barbieri, J. T. (2004) Ezrin/Radixin/Moesin Proteins Are High Affinity Targets for ADP-ribosylation by *Pseudomonas aeruginosa* ExoS. *J. Biol. Chem. 279* (37), 38402−38408.
(56) Sun, J., and Barbieri, J. T. (2003) *Pseudomonas aeruginosa* ExoT ADP-ribosylates CT10 Regulator of Kinase (Crk) Proteins. *J. Biol. Chem. 278* (35), 32794−32800.
(57) Barth, H., et al. (2004) Binary Bacterial Toxins: Biochemistry, Biology, and Applications of Common *Clostridium* and *Bacillus* Proteins. *Microbiol. Mol. Biol. Rev. 68* (3), 373−402.
(58) Vogelsgesang, M., Pautsch, A., and Aktories, K. (2007) C3 exoenzymes, novel insights into structure and action of Rho-ADP-

ribosylating toxins. *Naunyn-Schmiedeberg's Arch. Pharmacol. 374* (5), 347−360.
(59) Bulgin, R., et al. (2010) Bacterial guanine nucleotide exchange factors SopE-like and WxxxE effectors. *Infect. Immun. 78*, 1417−1425.
(60) Kenny, B., et al. (2002) Co-ordinate regulation of distinct host cell signalling pathways by multifunctional enteropathogenic *Escherichia coli* effector molecules. *Mol. Microbiol. 44* (4), 1095−1107.
(61) Schwan, C., et al. (2009) *Clostridium difficile* Toxin CDT Induces Formation of Microtubule-Based Protrusions and Increases Adherence of Bacteria. *PLoS Pathog. 5* (10), e1000626.
(62) Hilger, H., et al. (2009) The Long-Lived Nature of *Clostridium perfringens* Iota Toxin in Mammalian Cells Induces Delayed Apoptosis. *Infect. Immun. 77* (12), 5593−5601.
(63) Grant, C. C., Messer, R. J., and Cieplak, W. (1994) Role of trypsin-like cleavage at arginine 192 in the enzymatic and cytotonic activities of *Escherichia coli* heat-labile enterotoxin. *Infect. Immun. 62* (10), 4270−4278.
(64) Heine, K., et al. (2008) ADP-Ribosylation of Actin by the *Clostridium botulinum* C2 Toxin in Mammalian Cells Results in Delayed Caspase-Dependent Apoptotic Cell Death. *Infect. Immun. 76* (10), 4600−4608.
(65) Oh, S.-Y., et al. (2011) Two capsular polysaccharides enable *Bacillus cereus* G9241 to cause anthrax-like disease. *Mol. Microbiol. 80* (2), 455−470.
(66) Libby, S. J., et al. (2000) The *Salmonella* virulence plasmid spv genes are required for cytopathology in human monocyte-derived macrophages. *Cell. Microbiol. 2* (1), 49−58.
(67) Hernandez, E., et al. (1998) *Bacillus thuringiensis* subsp. konkukian (Serotype H34) Superinfection: Case Report and Experimental Evidence of Pathogenicity in Immunosuppressed Mice. *J. Clin. Microbiol. 36* (7), 2138−2139.
(68) McIntyre, L., et al. (2008) Identification of *Bacillus cereus* Group Species Associated with Food Poisoning Outbreaks in British Columbia, Canada. *Appl. Environ. Microbiol. 74* (23), 7451−7453.
(69) Kuroki, R., et al. (2009) Nosocomial Bacteremia Caused by Biofilm-Forming *Bacillus cereus* and *Bacillus thuringiensis*. *Int. Med. 48* (10), 791−796.
(70) Gibert, M., et al. (2011) Endocytosis and toxicity of clostridial binary toxins depend on a clathrin-independent pathway regulated by Rho-GDI. *Cell. Microbiol. 13* (1), 154−170.
(71) Pust, S., Barth, H., and Sandvig, K. (2010) *Clostridium botulinum* C2 toxin is internalized by clathrin- and Rho-dependent mechanisms. *Cell. Microbiol. 12* (12), 1809−1820.
(72) Nicasio, A. M., Kuti, J. L., and Nicolau, D. P. (2008) The Current State of Multidrug-Resistant Gram-Negative Bacilli in North America. *Pharmacotherapy 28* (2), 235−249.
(73) Davies, J., and Davies, D. (2010) Origins and Evolution of Antibiotic Resistance. *Microbiol. Mol. Biol. Rev. 74* (3), 417−433.
(74) Blaser, M. J., and Falkow, S. (2009) What are the consequences of the disappearing human microbiota? *Nat. Rev. Microbiol. 7* (12), 887−894.
(75) Luna, V. A., et al. (2007) Susceptibility of *Bacillus anthracis*, *Bacillus cereus*, *Bacillus mycoides*, *Bacillus pseudomycoides* and *Bacillus thuringiensis* to 24 antimicrobials using Sensititre® automated microbroth dilution and Etest® agar gradient diffusion methods. *J. Antimicrob. Chemother. 60* (3), 555−567.
(76) Turnbull, P. C. B., et al. (2004) MICs of Selected Antibiotics for *Bacillus anthracis*, *Bacillus cereus*, *Bacillus thuringiensis*, and *Bacillus mycoides* from a Range of Clinical and Environmental Sources as Determined by the Etest. *J. Clin. Microbiol. 42* (8), 3626−3634.